Photogrammetry based system for the measurement of cylindrical forgings axis straightness

Aneta Zatočilová[a*], Radek Polisčuk[a], David Paloušek[a], Jan Brandejs[a]

[a] Institute of Machine and Industrial Design, Faculty of Mechanical Engineering, Brno University of Technology, Technická 2896/2, 616 69 Brno, Czech Republic;

ABSTRACT

Dimension measurement of hot large forgings is necessary for manufacturing process and quality control. Conventional non-contact optical measurement methods are not applicable, mainly because of high temperature and large dimensions. A novel approach to the axis staightness measurement of the cylindrical forging, based on the principle of photogrammetry and edge detection, is described in this paper. Proposed system is developing under laboratory conditions, but the actual conditions of steel production are also considered. Demands on the measurement system were set by our industrial partner, producer of cylindrical forgings with length of 4 to 20 m and diameter up to 1.4 m. The system should be able to detect axis straightness deviations higher than 5 mm (system accuracy has to be better than 5 mm). Cylindrical forgings are 4 to 20 m long with diameter up to 1.4 m.

The approach is based on the assumption that the actual shape of the cylindrical forging axis can be determined (in the simplest case) using four boundary curves which lie in two mutually perpendicular planes. Four boundary curves can be obtained by detecting the forging´s edges in two images. The article provides results of first validation of proposed method in laboratory conditions. Measurement repeatability was validated by carrying out ten measurements of a deformed rod. Each measurement was compared with a measurement performed by industrial fringe projection scanner Atos III Triple Scan in order to verify the accuracy of the proposed method.

1. INTRODUCTION

Large forgings are semi-finished products which are used to manufacture components particularly for marine, nuclear and petrochemical industries. In the most cases, they have a simple cylindrical shape and usually are made by open die forging on a 10 000-ton hydraulic press at temperature range from 850 to 1300 °C. Control measurement and straightening on three-point press usually follows. This process is repeated until the forging shape deviations are within required limits. In the case of cylindrical forgings, demands are imposed particularly on the cylindricity and axis straightness. As the production of large forgings is very expensive, the demands on production efficiency still grow, simultaneously with demands on shape and dimensional accuracy of the forgings. This implies requirements on accurate, rapid and safe measurement.

In the present, many forging plants measure the forging dimensions by hand-held calipers or a mechanical gauge. An operator must be in the dangerous vicinity of the hot forging and only incomplete and inaccurate data are obtained in this way. Some automatic contact-based measurement systems were developed [1], but the implementation was not always successful due to their low-flexibility.

Ideally, the system should be non-contact, provide on-line measurement and real-time evaluation, i.e. without interrupting the production cycle. However, conventional non-contact optical measurement systems are not applicable due to large dimensions and high temperatures of measured parts. Optical measurement of hot parts also suffer from problems caused by: detection of IR rays emitted by the measured part; insufficient contrast of the projected pattern on the surface of the hot object; component dilatation of measurement device when working under high temperature; and different light infraction in the heat-affected area.

In the last decade, attention was paid to the development of specific non-contact optical systems that could overcome the above mentioned problems. The specific systems are based on different methods: laser scanning using time-of-flight

* zatocilova.a@fme.vutbr.cz, +420 541 143 216 ,+420 739 228 816

Optical Measurement Systems for Industrial Inspection VIII, edited by
Peter H. Lehmann, Wolfgang Osten, Armando Albertazzi, Proc. of SPIE Vol. 8788,
87881L · © 2013 SPIE · CCC code: 0277-786X/13/$18 · doi: 10.1117/12.2020917

method (TOF[2, 3]); laser scanning using triangulation method [4]; scanning with xenon light using triangulation method [5, 6], and imageing system based on photogrammetry principles [7-9]. Up to now, only the laser-based systems have been successfully implemented. However, very good results of experimental measurement carried out by fringe-projection scanner with xenon light were published in 2012 [10]. Scanners using TOF method are very expensive due to the cost of measurement equipment. On the other side, in the case of triangulation scanners may be problematic to ensure sufficient contrast of projected pattern. Studies on passive image-based methods, intended for the measurement of hot parts, are mainly focused on partial issues, such as edge detection, image acquisition act. Only Jian W. published experimental research in 2008, where optical system based on CCD imaging was used to measure small cylindrical parts under high temperature [11].

When the axis straightness has to be measured, complex data on the shape of the forging are not necessary. The image-based methods are not able to acquire overall information about shape. However, it could be simple, reliable and not very expensive solution for the non-contact measurement of forging axis straightness.

2. IMAGE-BASED SYSTEM CONFIGURATION

The proposed approach is based on the assumption that the actual shape of the cylindrical forging axis can be determined (in the simplest case) from the four boundary curves, that lie in two mutually perpendicular planes (fig. 1). Four boundary curves can be obtained by detecting forging edges in the two images.

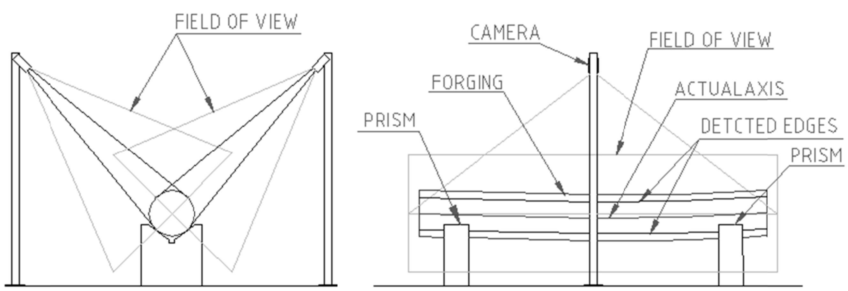

Figure 1. Image-based system configuration with two cameras.

Selecting appropriate camera and lens is the basic requirement for image-based system measurement. Accuracy of the system is determined by relative precision (minimum detectable size) and measurement deviations, such as deviations resulting from edge detection and deviations resulting from the optical system, which cannot be eliminated by calibration etc. In case of optical systems, the relative precision is dependent on resolution of the image. The imaging resolution is dependent on sensor resolution and dimensions of the measured area. It increases with the decreasing field of view, but this approach would also decrease the measured forging dimensions. When the forging is longer than the visible area, more cameras can be used in parallel configuration (fig. 2) and the resulting panoramic image can be processed. However, using multiple cameras also increases the price of the system.

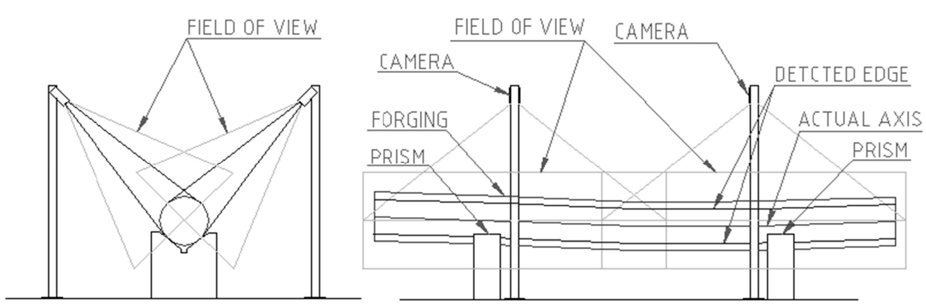

Figure 2. Image-based system with parallel configuration.

Differentiation of equation (1) shows that the uncertainty of an image measurement dx' can be transferred into object space by the image scale number m [12]:

$$dX = m \cdot dx' \tag{1}$$

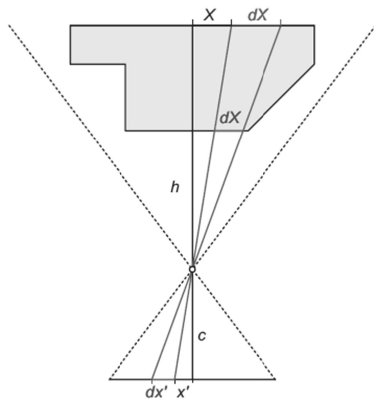

Figure 3. Single image acquisition [12].

In many cases a relative precision that is related to the maximum object dimension S or the maximum image format *s´* is calculated [12]:

$$m = \frac{s_x}{S} = \frac{s_x{}'}{s'} \tag{2}$$

The image scale number *m* is defined by the ratio of object distance *h* to the principal distance *c* (lens focal length with the addition of an extension in order to achieve sharp focus) of the camera system used. It may also be given as the ratio of a distance in object space *X* to the corresponding distance in image space *x*' [12]:

$$m = \frac{h}{c} = \frac{X}{x} \tag{3}$$

3. LABORATORY MEASUREMT

3.1 Measurement equipment and parameters

The first phase of the development was focused on optimizing and testing the methodology for measuring cold cylindrical rods. For this purpose, rods with length of 700 mm and diameter of 45 mm were used. A measurement stand was constructed for two digital cameras Canon EOS 500D with a resolution of 18Mpix (figure 4). Size of camera´s image sensor is 22.3x14.9 mm^2 (x_{max}=22.3 mm, y_{max}=14.9 mm) and pixel size is 4.69×4.70 μm^2 ($s_x{}'$=0.00470 mm, $s_y{}'$=0.00469 mm). Distance of the cameras focal ceter from the object plane was calculated for focal length f=18 mm and length of field of view 800 mm (X_{max}=800 mm) according to the equation 3; relative precision was computed according to the equation 2:

$$m = \frac{X_{max}}{x_{max}} = \frac{800}{22,3} = 35,87$$

$$h = m \cdot c = 35,87 \cdot 18 \cong 638\, mm$$

$$s_X = m \cdot s_x{}' = 35,87 \cdot\ 0,00470 = 0,1686\, mm \cong 0,17\, mm$$

The cameras are mounted on a lift, in order to make their position adjustable in the vertical direction. The Angle between the camera image planes is approximately 90°. The measured rod is placed approximately in the middle of the scene onto two prisms. Since edge detection method will be used, background of the rod has to provide enough contrast. The scene with cameras and sample rod is shown in figure 4.

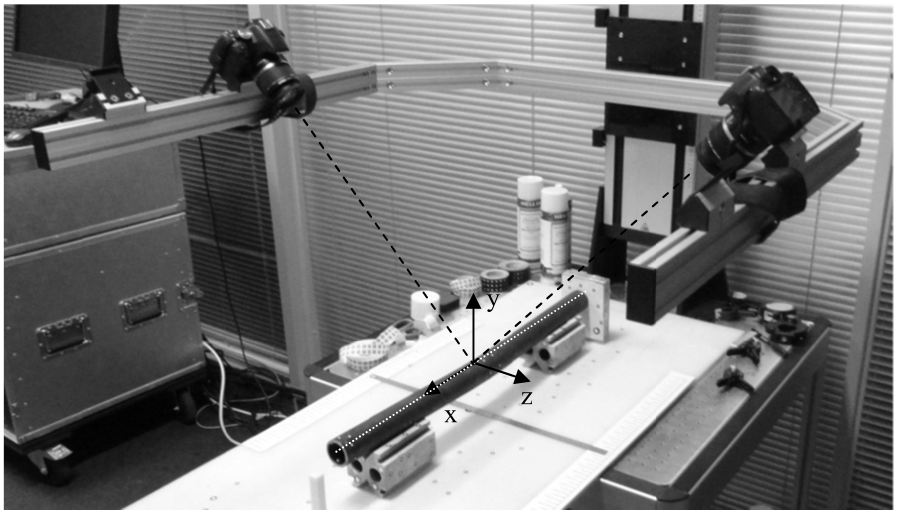

Figure 4. Configuration of laboratory measurement system.

3.2 Camera calibration

Camera calibration should be performed for the actual measurement conditions, i.e. in the actual working distance, chosen focal length and aperture. Metric calibration is usually based on the comparison of the markers' position in a distorted image with their true position, which is usually performed by imaging of the calibration panel. Panel with regularly distributed markers should match the size of the field of view in the working distance. Due to the fact that the field of view of the proposed system is very large (if real conditions are considered), the calibration should be simplified to 1D issue. 1D calibration (with one-directional field of markers) was performed using a tape measure (figure 5). Tape measure was thoroughly stretched in horizontal direction across the whole field of view. Position above the table was adjusted, so that tape measure laid at ideal axis between the edges of the measured rod. Vertical position of cameras was adjusted so that the horizontal axis of the image plane approximately corresponds to the middle line of the tape measure. Calibration was performed using a single image taken from the working position of each camera. In the image, number of pixel between every 10 mm markers on the tape measure was determined. Fig. 5 shows image with mesh that represents radially symmetric distortion of actual imaging system. The software then rectifies all relative pixel coordinates, in order to obtain real correct metric coordinates at relevant image plane.

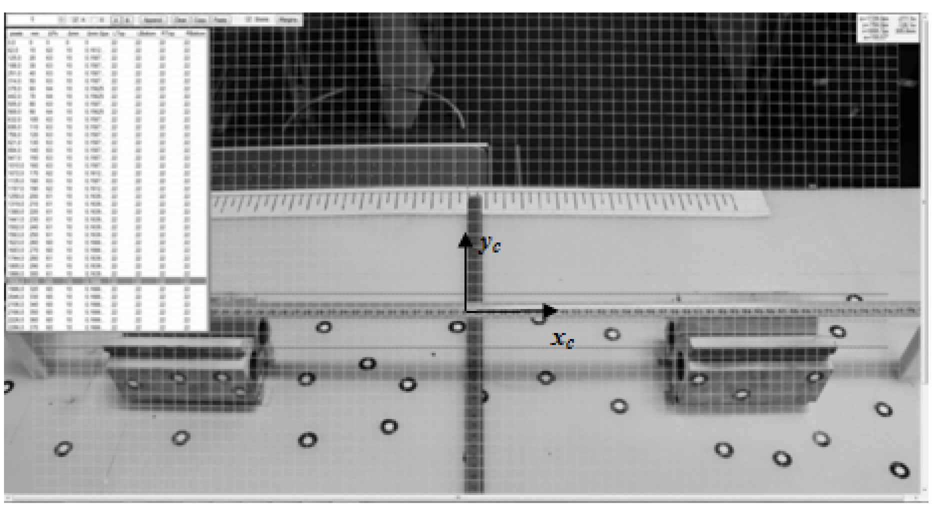

Figure 5. Image A: scene with mesh that represents radially symmetric distortion.

The table 1 shows deviations caused by radial distortion; in the vicinity of the optical axis, the pixel size (Δmm/Δpx) corresponds to calculated relative precision.

Table 1. Evaluation of deviations caused by radial distortion: mm - actual position of the markers in (mm), Δpx number of pixels between markers, Δmm – actual distance of markers in (mm), Δmm/Δpx - pixel size between markers in (mm).

	Calibration - camera A					Calibration - camera B				
Section no.	px	mm	Δpx	Δmm	Δmm/ Δpx	px	mm	Δpx	Δmm	Δmm/ Δpx
1	0	0	0	0	0	0	0			
2	62	10	62	10	0,1613	62	10	62	10	0,1612
3	125	20	63	10	0,1587	125	20	63	10	0,1587
4	188	30	63	10	0,1587	188	30	63	10	0,1587
5	251	40	63	10	0,1587	251	40	63	10	0,1587
….	….	….	….	….	….	….	….	….	….	….
35	2166	350	60	10	0,1666	2166	350	60	10	0,1678

The next step is calibration of the internal parameters of linear imaging system, i.e. the calculation of the position and orientation of the image plane. Exact angle of the cameras and their distance from the object plane was calculated using vertical (H) and horizontal gauge (M).

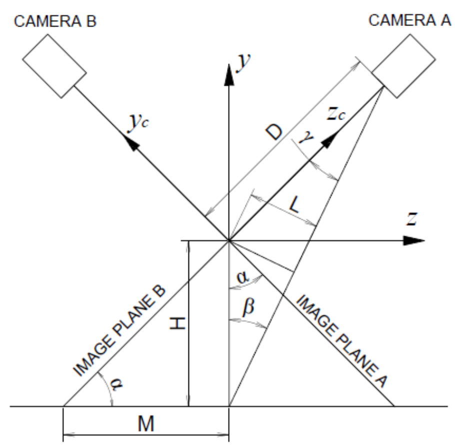

Figure 6. Calibration diagram. Cameras´ coordinate system - red color, global coordinate system - black color.

Table 2. Calibration of linear internal parameters of cameras using gauges and tape measure.

	Camera A	**Camera B**	
L [mm]	55.1	54.1	Projection of the tables´ centre line to the image planes
M [mm]	84.6	81.6	Projection of the tapes´ centre line to the table
H [mm]	87.0	87.0	Distance of the tapes´ centre line above the table

Actual rotation of optical axis z_c and y_c (image A and B) from the object axis z and other auxiliary angles were determined using known dimensions of the scene in three directions:

$$\alpha = arctan\left(\frac{H}{M}\right) \tag{4}$$

$$\beta = arctan\left[\frac{(L \times sin\alpha)}{(H - L \cdot cos\alpha)}\right] \tag{5}$$

$$\gamma = 90 - \alpha - \beta \tag{6}$$

Distance between intersection of the principal axis and image planes (see figure 6):

$$D = \frac{L}{\tan\gamma} \tag{7}$$

Table 3. Results of internal camera calibration: orientation of cameras and their distances form object planes.

	Camera A		**Camera B**		
	[rad]	[deg]	(rad)	[deg]	**Description**
α	0.803	46,0	0.817	46.8	Angle between principal axis and z direction
β	0.683	39.1	0.668	38.29	Angle between central point of the table, projected to the image plane and z direction
γ	0.085	4.88	0.085	4.88	Angle between principal axis and central point of the table projected to the image plane
D	625.9 mm		624.3 mm		Distance between the intersection of the principal axis and focal centre

3.3 Edge detection method and data evaluation

A crucial step for the function of the proposed system is choice of the edge detection method, which will ensure precise extraction of the forging's boundary curves. The chosen method has to be appropriate for measurement of the hot and normal temperature forgings, which is not an easy task. Common edge detection methods extract edges in the whole image, however, in this issue only two boundary curves are required. The method evaluates the luminance (L*) values around the analyzed cross section cuts using short horizontal median filter, in order to obtain values not affected by local impulse noise, marks and scratches in the raw image. The edge itself is then detected as steepest vertical L* gradient at direction given by local coordinate system. Figure 7 shows that edge detection fails in the area of prisms, where the contrast between the rod and the background is insufficient. Therefore, the width of the prisms should be minimized.

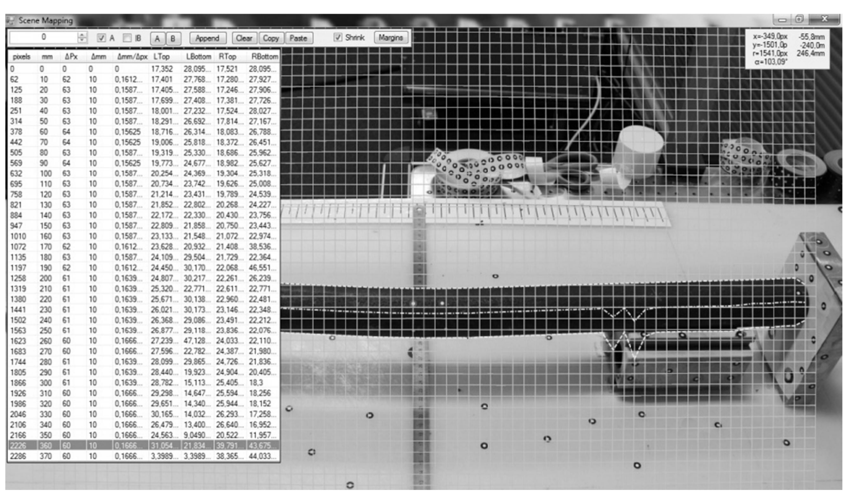

Figure 7. Edge detection and user interface of the proposed system.

The figure 8 shows the key parameters – maximum deflection ***d***, it´s distance ***l*** from the right end point and angle $\boldsymbol{\theta}$ between vector of maximum deflection and z direction. The maximum deflection is computed as a distance of actual axis (points C) to the ideal reference axis (points C_{ref}). The reference axis is constructed using mid points that lie in the cross sections at both ends of the rod, i.e. these mid points are the same for the actual and reference axes (see fig. 8).

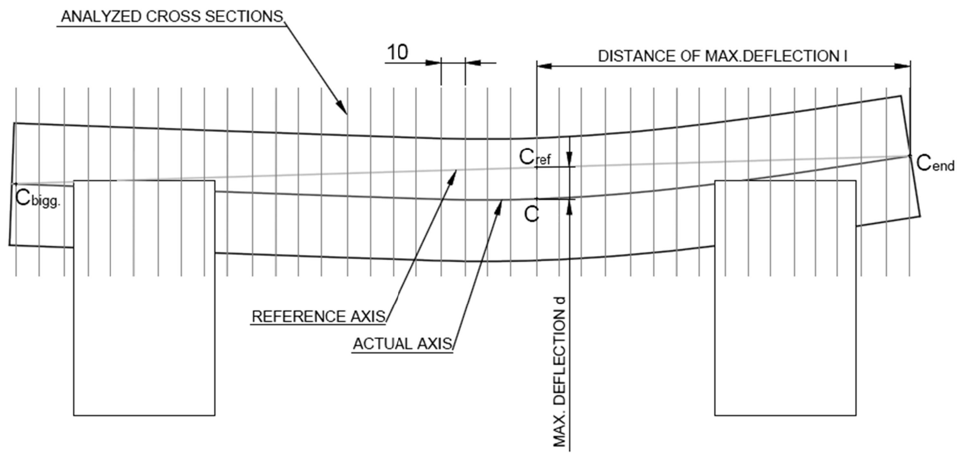

Figure 8. Measured parameters – maximum deflection ***d*** and a distance of maximum deflection ***l***.

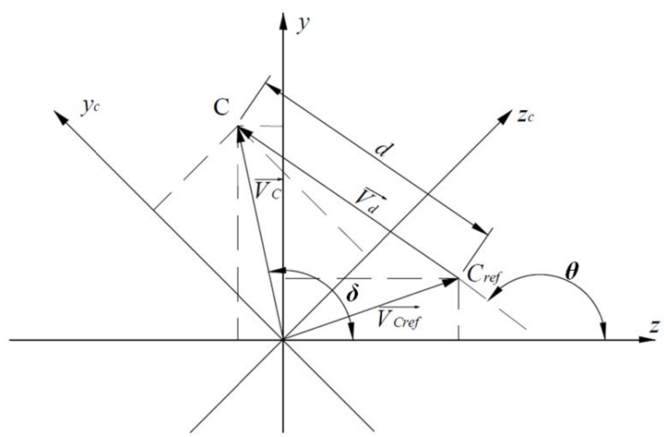

Figure 9. Vectors of actual and reference points *C*, maximum deflection *d* and corresponding angles. Camera coordinate system x_c, y_c, z_c; global coordinate system *x, y, z*; $(x_c = x)$.

The figure 9 shows angles and vectors computed according to the following steps:

1. Software was designed to detect boundary points (index top and bottom) for each image A and B in the vertical cross sections for every 10 mm:

$$y_c(x_c),\ z_c(x_c) \ \text{ for } x_c = -N...N,\ N=35 \tag{8}$$

$$A_{top} = +y_c(x_c),\ A_{bott} = -y_c(x_c) \tag{9}$$

$$B_{top} = +z_c(x_c),\ B_{bott} = -z_c(x_c) \tag{10}$$

2. Distances of two boundary points from the horizontal optical axis x_c ($x_c = x$) are used to calculate middle points:

$$A_{mid}(x_c) = \frac{A_{top} + A_{bott}}{2}, B_{mid}(x_c) = \frac{B_{top} + B_{bott}}{2} \tag{11}$$

3. Points C that lie on the actual axis of the rod were computed using middle points' coordinates relative to the cameras coordinate system. Size of the vector $\boldsymbol{V_C}$ was computed:

$$\boldsymbol{V_C} = (A_{mid}, B_{mid}) \tag{13}$$

$$\|\boldsymbol{V_C}\| = \sqrt{(A_{mid})^2 + (B_{mid})^2]} \tag{14}$$

4. Angle $\boldsymbol{\delta}$ of the vector $\boldsymbol{V_C}$ relative to the global axis $\boldsymbol{z}$ (see figure 9), was computed according to the following table.

Table 4. Table of quadrants for computation of angle δ.

y_c	z_c		δ [°]
$= 0$	> 0		45
	< 0		225
< 0	$= 0$		315
> 0			135
< 0	< 0		$315 - arctan\frac{y_o}{z_o}, \quad \delta \in < 225; 315 >$
	> 0	$arctan\frac{y_o}{z_o} < 45$	$315 - arctan\frac{y_o}{z_o}, \quad \delta \in < 315; 0 >$
		$arctan\frac{y_o}{z_o} > 45$	$-45 - arctan\frac{y_o}{z_o}, \quad \delta \in < 0; 45 >$
> 0	< 0		$135 - arctan\frac{y_o}{z_o}, \quad \delta \in < 135; 225 >$
	> 0		$135 - arctan\frac{y_o}{z_o}, \quad \delta \in < 45; 135 >$

5. Coordinates of the points C relative to the global coordinate system:

$$c_z = \|\boldsymbol{C}\| \cdot cos\,\delta \tag{15}$$

$$c_y = \|\boldsymbol{C}\| \cdot sin\,\delta \tag{16}$$

6. Vector of the reference axis was computed using middle points that lie in the cross sections at both ends of the rod:

$$\boldsymbol{V_{Cref}} = C_{end}[x, y, z] - C_{bigg}[x, y, z] \tag{16}$$

7. Determination of coordinates of the points C_{ref} that lie on the planes which are normal to the reference axis and intersect corresponding points C.

8. Deflection d was computed as the distance of the actual axis to the reference axis for each cross section:

$$\boldsymbol{V_d} = C_{ref}[x, y, z] - C[x, y, z] = (v_x, v_y, v_z) \tag{18}$$

$$d = \|\boldsymbol{V_d}\| \tag{19}$$

9. Finally, angle ϵ, which defines rotation of the vector $\boldsymbol{V_d}$ was used to compute angle θ of the maximum deflection relative to the z direction according to the table 5:

$$\varepsilon = arctg\frac{v_y}{v_z} \tag{18}$$

Table 5. Table of quadrants for computation of angle θ.

v_y	v_z	Θ
> 0	> 0	$\Theta=\epsilon$
> 0	< 0	$180 + \epsilon$
< 0	> 0	$360 + \epsilon$
< 0	< 0	$180 + \epsilon$

3.4 Measurement verification

Measurement repeatability was validated by carrying out ten measurements of deformed rod. Rotation of the rod was changed for each measuremet. Each measurement was compared with measurement performed by industrial fringe projection scanner Atos III Triple Scan [13] in order to verify the accuracy of the proposed method. Point spacing distance of Atos with 320 measurement volume (i.e. 320 x 240 x 240 mm^2) is 0.104 mm. Accuracy of the Atos measurement system is 0.003 mm according to acceptance protocol that complies with standard VDI/VDE 2634. Next table shows results of ten measurements.

Table 6. Results of the measurement.

<table>
<tr><th></th><th colspan="3">Size of max. deflection d [mm]</th><th colspan="3">Angle of max. deflection θ [°]</th><th colspan="2">Position of max. deflection l [mm]</th></tr>
<tr><th>Sample no.</th><th>Atos III Triple Scan</th><th>Proposed system</th><th>Deviation from the Atos</th><th>Atos III Triple Scan</th><th>Proposed system</th><th>Deviation from the Atos</th><th>Atos III Triple Scan</th><th>Proposed system</th></tr>
<tr><td>1</td><td rowspan="10">12.28</td><td>12.56</td><td>-0.28</td><td>339</td><td>338.8</td><td>0.2</td><td rowspan="10">352.7</td><td rowspan="10">cross section no. 0
350
±10</td></tr>
<tr><td>2</td><td>12.20</td><td>0.08</td><td>29.4</td><td>28.9</td><td>0.5</td></tr>
<tr><td>3</td><td>12.58</td><td>-0.3</td><td>92</td><td>93.6</td><td>-1.6</td></tr>
<tr><td>4</td><td>12.15</td><td>0.13</td><td>122.5</td><td>124.0</td><td>-1.5</td></tr>
<tr><td>5</td><td>12.49</td><td>-0.21</td><td>164.9</td><td>166.9</td><td>-2.0</td></tr>
<tr><td>6</td><td>12.28</td><td>0</td><td>216.4</td><td>214.8</td><td>1.6</td></tr>
<tr><td>7</td><td>12.35</td><td>-0.07</td><td>259.6</td><td>261.9</td><td>-2.3</td></tr>
<tr><td>8</td><td>12.12</td><td>0.16</td><td>318.6</td><td>320.7</td><td>-2.1</td></tr>
<tr><td>9</td><td>12.47</td><td>-0.19</td><td>11.4</td><td>10.0</td><td>1.4</td></tr>
<tr><td>10</td><td>12.28</td><td>0</td><td>65.9</td><td>64.3</td><td>1.6</td></tr>
</table>

4. CONCLUSION

This paper presents an approach to the axis straightness measurement of cylindrical forgings and shows results of the first experimental measurement in laboratory conditions. The proposed image-based system is based on the assumption that actual shape of the cylindrical forging axis can be determined (in the simplest case) using four boundary curves, that lie in two mutually perpendicular planes. The measurement approach was tested in laboratory conditions on the cylindrical rod sample of room temperatures with length of 700 mm and diameter of 45 mm. Results of image-based measurement ware compared with results of measurement by industrial 3D scanner Atos III Triple Scan. Table 6 shows that difference between results of both measurements methods. Deviation of maximum deflection size is less than 0.3 mm; deviation of angle is less than 3°. If the corresponding deviation is applied on 11 meters long field of view, the deviation of the deflection size equals to 4 mm. This meets the producer requirement for or the forging error range of ±5mm.

In real conditions, measurement system would be equipped with industrial cameras, which are thermally resistant, robust construction, monochrome, without integral IR filter. For example, industrial monochrome cameras JAI AM-1600 GE or Allied Vision Technology Pike F-1600 with Kodak KAI-16000 image sensor have resolution 16 Mpix (4872x3248 pixels, pixel size of 7.4 × 7.4 mm). Monochromatic cameras provide typical resolution up to 2× higher than color cameras, due to absence of Bayer mask over single chip sensor.

The critical condition of the presented measurement method was precise adjustment of the cameras, in order to keep the horizontal image axes parallel to the ideal reference axis. Despite the positive forecasts, additional measurements must be performed to determine the repeatability of the measurement on different sized samples. Further work will be devoted to testing and optimizing the measurement of hot forgings.

5. ACKNOWLEDGMENTS

The work was supported by European Regional Development Fund in the framework of the research project NETME Centre under the Operational Programme Research and Development for Innovation. Reg. Nr. CZ.1.05/2.1.00/01.0002, id code: ED0002/01/01, project name: NETME Centre – New Technologies for Mechanical Engineering.

6. REFERENCES

[1] Nye, T. J., Elbadan, A. M. and Bone, G. M. "Real-time process characterization of open die forging for adaptive control". ASME Journal of Engineering Materials and Technology, 123(4), 511–516 (2001).

[2] [2] MITEQ, "FERROTRON A MINTEQ DIVISION," c2011, < http://www.minteq.com/fileadmin/user_upload/minteq/PDF/M-FE-30-PDF-Forge__Jan2011_.pdf > (16 July, 2012)

[3] MERMEC GROUP, "MERMEC GROUP," c2009, < https://www.mermecgroup.com/download.php?f=/mermec-incorso/images/File/newsletter/InsightSteel_vol1_n1_eng.pdf. > (16 July 2012)

[4] SINTEF. "SINTEF" 2008. Measuring 3D shape of steel shafts during forging. < http://www.sintef.no/home/Information-and-Communication-Technology-ICT/Optical-measurement-systems-and-data-analysis-/Projects/Measuring-3D-shape-of-steel-shafts-during-forging/ > (16 July 2012)

[5] Jia, Z. at al. "An improved image acquiring method for machine vision measurement of hot formed parts," Journal of Materials Processing Technology, 210(2), 267-271 (2010)

[6] Liu, W. at al. "Fast dimensional measurement method and experiment of the forgings under high temperature," Journal of Materials Processing Technology, 211(2), 237–244 (2011)Chaudhuri, S. at al. “Automatic measurement of frontal area and volume of fluted ingots using image-based instrumentation,” Measurement, vol. 33 (no. 4), 325-332 (2003)

[7] Chaudhuri, S. at al. "Automatic measurement of frontal area and volume of fluted ingots using image-based instrumentation," Measurement, 33(4), 325-332 (2003)

[8] Dworkin, S. B. and Nye T.J. Image processing for machine vision measurement of hot formed parts, "Journal of materials processing technology," 174(1), 1-6 (2006)

[9] Hu, CH., Liu, B. and Song, X, "A novel edge detection approach used for online dimensional measurement of heavy forging," Proc. SPIE 7160, 110-119 (2008)

[10] Liu, W. at al. "An improved online dimensional measurement method of large hot cylindrical forging," Measurement, 45(8), 2041-2051 (November 16 2012)

[11] Juan, W., Zurona, Q. and Jin, L. "Experimental research on dimensional measurement of hot parts based on CCD," Proc. SPIE 6829, (November 26, 2007).

[12] Luhmann, T., et al. "Image scale and accuracy" [Close Range Photogrammetry: Principles, techniques and applications] Whittles Publishing, Dunbeath, Caithness KW6 6EG, Scotland,UK,100-104 (2011)

[13] GOM, "GOM: Optical Measurement Techniques," < http://www.gom.com/> (28 July 2011)